ACS OMEGA

Article

Cite This: ACS Omega 2018, 3, 5980−5987

Self-Assembly of a Dentinogenic Peptide Hydrogel

Peter K. Nguyen,[†] William Gao,[†] Saloni D. Patel,[†] Zain Siddiqui,[†] Saul Weiner,[§] Emi Shimizu,[∥] Biplab Sarkar,*[,†] and Vivek A. Kumar*[,†,‡,§]

[†]Department of Biomedical Engineering and [‡]Department of Chemical, Biological and Pharmaceutical Engineering, New Jersey Institute of Technology, Newark, New Jersey 07102, United States

[§]Department of Restorative Dentistry and [∥]Department of Oral Biology, Rutgers School of Dental Medicine, Newark, New Jersey 07103, United States

ABSTRACT: Current standard of care for treating infected dental pulp, root canal therapy, retains the physical properties of the tooth to a large extent, but does not aim to rejuvenate the pulp tissue. Tissue-engineered acellular biomimetic hydrogels have great potential to facilitate the regeneration of the tissue through the recruitment of autologous stem cells. We propose the use of a dentinogenic peptide that self-assembles into β-sheet-based nanofibers that constitute a biodegradable and injectable hydrogel for support of dental pulp stem cells. The peptide backbone contains a β-sheet-forming segment and a matrix extracellular phosphoglycoprotein mimic sequence at the C-terminus. The high epitope presentation of the functional moiety in the self-assembled nanofibers may enable recapitulation of a functional niche for the survival and proliferation of autologous cells. We elucidated the hierarchical self-assembly of the peptide through biophysical techniques, including scanning electron microscopy and atomic force microscopy. The material property of the self-assembled hydrogel was probed though oscillatory rheometry, demonstrating its thixotropic nature. We also demonstrate the cytocompatibility of the hydrogel with respect to fibroblasts and dental pulp stem cells. The self-assembled peptide platform holds promise for guided dentinogenesis and it can be tailored to a variety of applications in soft tissue engineering and translational medicine in the future.

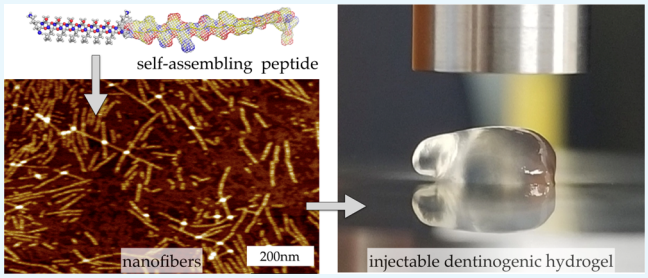

INTRODUCTION

Ninety-one percent of adults in the United States between the ages of 20 and 64 have caries in their nondeciduous teeth due to factors such as bacterial infection and physical injury.[1] Normally, these dental cavities can be treated with routine restorative procedures. However, in the cases of severe caries, the entire dental pulp may be infected and cannot be preserved.[2] Currently, the standard treatment in these circumstances is to completely extirpate the infected pulp, disinfect the root canal, and fill it with elastomeric materials (such as gutta percha). This root canal therapy results in a devitalized tooth that is devoid of a cellular niche or vasculature.[2] The elastomeric materials cannot intrinsically prevent recontamination, for example, bacterial colonies can extend into apical tissues through apical foramen, resulting in apical periodontitis.

Deterioration of enamel and dentin in the damaged teeth may lead to formation of fibrin-based clots in the dental cavities. These clots readily resorb in less than 3 days, leaving cavities that remain dormant till future insult. Regeneration of pulplike tissue in these cavities after clinical extirpation is extremely consequential for regenerative endodontics. Unguided regeneration of periapical tissue distinct from pulp, mediated by a fibrin scaffold with entrapped platelets and red blood cells, was achieved over 50 years ago.[3−5] Next generation scaffolds attempted in situ pulp regeneration with biologically or synthetically derived materials, such as collagen matrices and other hydrogels.[5] However, hypoxia, necrosis, and the essential lack of a physical support have limited these potential therapeutic approaches thus far. Concerns with cell source and off-the-shelf availability of cell-loaded constructs have hindered cell-based therapies. Despite the investigation of several promising therapeutic avenues in the last few decades, no therapies for regeneration of dental pulp tissue have been approved by the FDA to date.[6−9]

Introduction of a slowly degrading biomaterial that fosters cellular ingrowth without fibrous encapsulation is a key requirement for viable tissue regeneration. As cells proliferate, scaffolds need to provide a niche that is not only conducive to extracellular matrix (ECM) production and deposition but is also potentially instructive to determine the phenotype of infiltrating cells. The infiltration of stem cells into ECM-mimetic nanofibrous scaffolds and directed differentiation into dentin-producing cells may enhance vital pulplike tissue regeneration. We hypothesize that instructive cues within scaffolds may promote infiltration of autologous stem cells from surrounding tissues and their niche-specific differentiation.

Received: February 26, 2018
Accepted: May 2, 2018
Published: June 4, 2018

DOI: 10.1021/acsomega.8b00347
ACS Omega 2018, 3, 5980−5987

PEPTIDE DESIGN AND NANOFIBROUS SELF-ASSEMBLY

Postnatal dental pulp stem cells (DPSCs) differentiate into odontoblast-like cells during pulp injury, which are believed to play a crucial role in forming reparative dentin. Liu et al. reported that dentonin, a bioactive portion of matrix extracellular phosphoglycoprotein (MEPE), has a potential role in pulp repair via its ability to promote DPSC proliferation.[10] Six et al. postulated from their research that the initial cascade of events leading to pulp healing are primarily affected by this bioactive portion.[11] Dentonin (TDLQERGDNDISPFSGDGQPFKD) possesses both the RGD integrin-binding motif and the SGDG glycosaminoglycan-binding motif of MEPE. Researchers have shown that both of these motifs are required for bioactivity, and thus dentonin has the potential to assist the survival of injured pulp. In this work, we will explore the attachment of dentonin to a self-assemble peptide framework for possible therapeutic application (Table 1).

Table 1. Peptide Sequences Studied in This Article[a]

Name	Sequence
[A]SLd	KSLSLSLSLSLSLK-G-TDLQERGDNDISPFSGDGQPFKD
[B]SLd^{mod}	KSLSLSLSLSLSLK-G-SEFNDKPEQEFTGLQPDPSGIRE
[C]SL-base	KSLSLSLSLSLSLK

[a]All sequences are N-terminally acetylated and C-terminally amidated. (A) Dentonin, a MEPE mimic, is highlighted in green in the sequence of the main therapeutic candidate, SLd. (B) SLd^{mod} is a control sequence with similar polarity to SLd but contains an altered primary sequence (changed amino acids shown in red). (C) Both peptides are based on the sequence of SL-base, which has a sequence similar to a previously characterized self-assembling peptide.[12−14]

Self-assembling peptide hydrogels (SAPHs) are created from multidomain peptides, which have 12−50 amino acid primary sequences with repeating hydrophobic and hydrophilic residues and can be triggered to self-assemble in aqueous solution to form nanofibers with β-sheet secondary structure.[9,15−18] Self-assembly is mediated by bonds that break and reassemble reversibly: hydrogen bonding, van der Waals interactions, and ionic interactions. These afford thixotropic rheological properties: rapid shear thinning and shear recovery.[9,17] Therefore, these hydrogels can be easily syringe aspirated, injected, and reassembled in situ to provide a prolonged, sustained biological response. The general self-assembly platform has been evaluated for drug delivery, angiogenesis, inflammation modulation, and recovery from ischemic tissue disease.[16−20] At the ultrastructural level, these peptides self-assemble into biomimetic nanofibers. The nanofibrous architecture is crucial for supporting cells in vivo, and the presentation of bioactive domains on such nanofibers have been shown to be instructive for infiltrating cells.[17,21] Rational design of these injectable ECM-mimetic scaffolds may be directed toward facilitating infiltration and phenotypic modulation of surrounding cells.[18,22] For example, a mimic of vascular endothelial growth factor-165 (VEGF-165) was engineered into a similar β-sheet-forming peptide sequence for promoting robust angiogenesis in vitro and in vivo.[17,20] These hydrogels have shown rapid improvement in reperfusion of ischemic limbs in mice with femoral artery ligation.[20]

Thus, attachment of a functional bioactive mimic to the SAPH platform may potentially lead to biological and physical properties required for tissue remodeling and regeneration. In this article, we explore the use of dentonin to modify the sequence of a parent SAPH system (SL-base, Table 1) to design a new hybrid peptide, SLd, to achieve a dentinogenic outcome (Table 1). The functionalized peptide is expected to form β-sheet-based nanofibers (Scheme 1A−C) and indeed forms a stable hydrogel in aqueous solution (Scheme 1D,E), indicating the possibility of nanofibers as constituents. However, we need further biophysical characterization to prove the self-assembly of nanofibers. To determine the importance of the functional domain (dentonin), we designed a control peptide (SLd^{mod}, Table 1) with a similar polarity to SLd, but containing an altered sequence. A crucial aspect of the design is that the dentonin functionality is displayed at the edge of the nanofiber at a high epitope density, enable facile signaling mechanism similar to MEPE.

RESULTS AND DISCUSSION

Around 15 million root canal procedures are completed in the US every year. The infected pulp is removed and replaced with inert elastomeric materials, such as gutta percha. The resulting devitalized tooth does not have any regenerative potential. The current exploratory pulp-capping treatments (calcium hydroxide, mineral trioxide aggregate, biodentine, etc.) do not offer a solution to this fundamental problem.[23] Here, we propose the use of regenerative peptide scaffolds as a potential therapeutic solution (Scheme 2). There are multiple challenges in designing such biomaterials. For example, (a) the material needs to be easily deliverable to the targeted tissue niche. Moreover, (b) the hydrogel or scaffold should be nontoxic and should be able to support autologous cells in the pulpal niche. Another important criterion is (c) a proper biodegradability profile: rapid degradation of the material may limit support of autologous cells in vivo for the required regeneration and very slow degradation may hinder the gradual replacement of the construct by the native deposited matrix. In this article, we report significant advancement toward the first two goals.

Self-Assembly. The target peptide with the dentonin functional moiety, SLd (Table 1), was dissolved in 298 mM sucrose and combined with a molar equivalent of calcium chloride ($CaCl_2$). Consistent with the self-assembly scenario in Scheme 1, SLd forms a robust hydrogel. The ultrastructure of the hydrogel was determined through scanning electron microscopy (SEM) and atomic force microscopy (AFM) (Figure 1). Critical point-dried samples of SLd show a nanofibrous meshlike morphology in SEM. In terms of fiber density and alignment, these nanofibers are comparable to self-assembled peptides reported before.[17] Through AFM, we determined the height (~2 nm) and width (~14 nm) of these ribbonlike nanofibers, which is again consistent with the ribbonlike self-assembly, depicted in Scheme 1.

Viscoelasticity. Through oscillatory rheometry, we determined that the viscoelastic properties of the SLd hydrogel (G' > 100 Pa) (Figure 2) are comparable in magnitude to similar self-assembled peptide hydrogels.[17,18] Crucially, the hydrogel undergoes liquefaction under shear force and immediately recovers its storage modulus when the force is removed. Quantitatively, when the hydrogel experiences high shear strain (100% strain), the storage modulus (G') of the hydrogel drops

DOI: 10.1021/acsomega.8b00347
ACS Omega 2018, 3, 5980−5987

Scheme 1. Peptide Self-Assembly and Gross Hydrogel Structure[a]

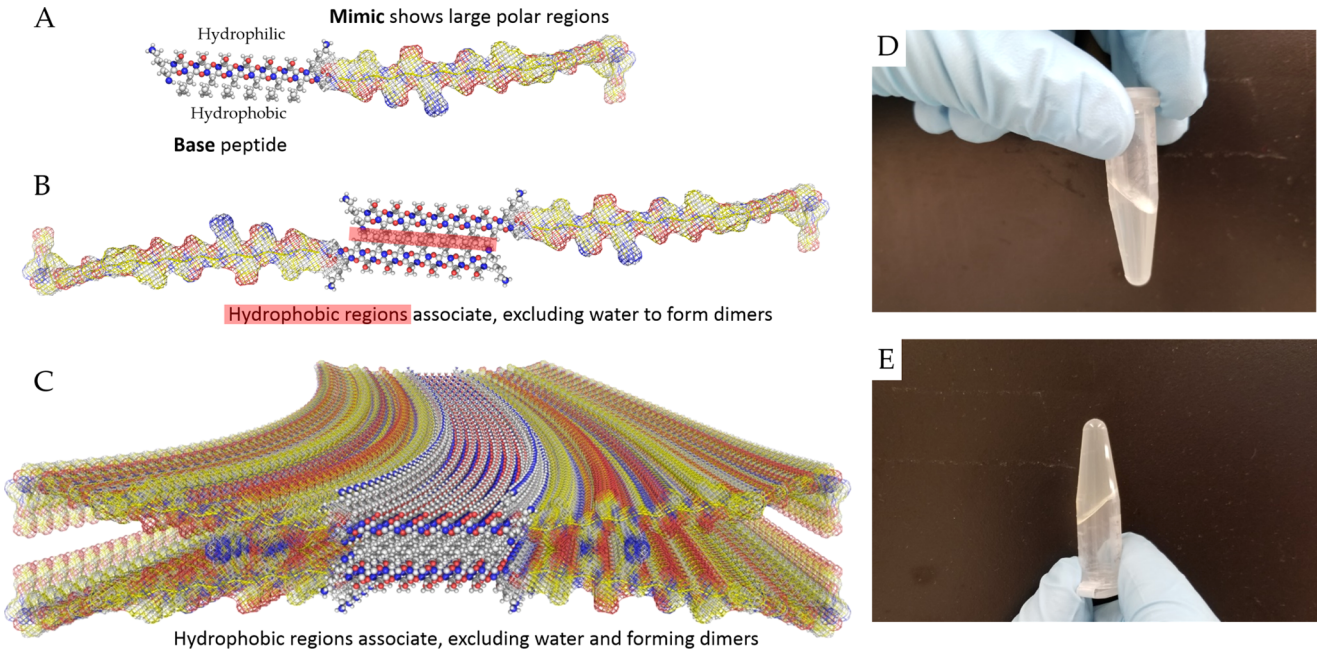

[a](A–C) The base sequence has alternative hydrophilic and hydrophobic residues. In aqueous media, the hydrophobic leucine residues collapse into a core, exposing the hydrophilic serine residues to the surface. Stacking of a tetrameric unit to maximize hydrogen bonding leads to the formation of a β-sheet nanofiber. The lengthening and crosslinking of the nanofibers is favored in physiological salt concentrations as the repulsion among the positively charged lysine residues is shielded, leading to (D, E) the formation of robust hydrogels that maintain their shape.

Scheme 2. Injectable Peptide Scaffolds for Pulpal Regeneration[a]

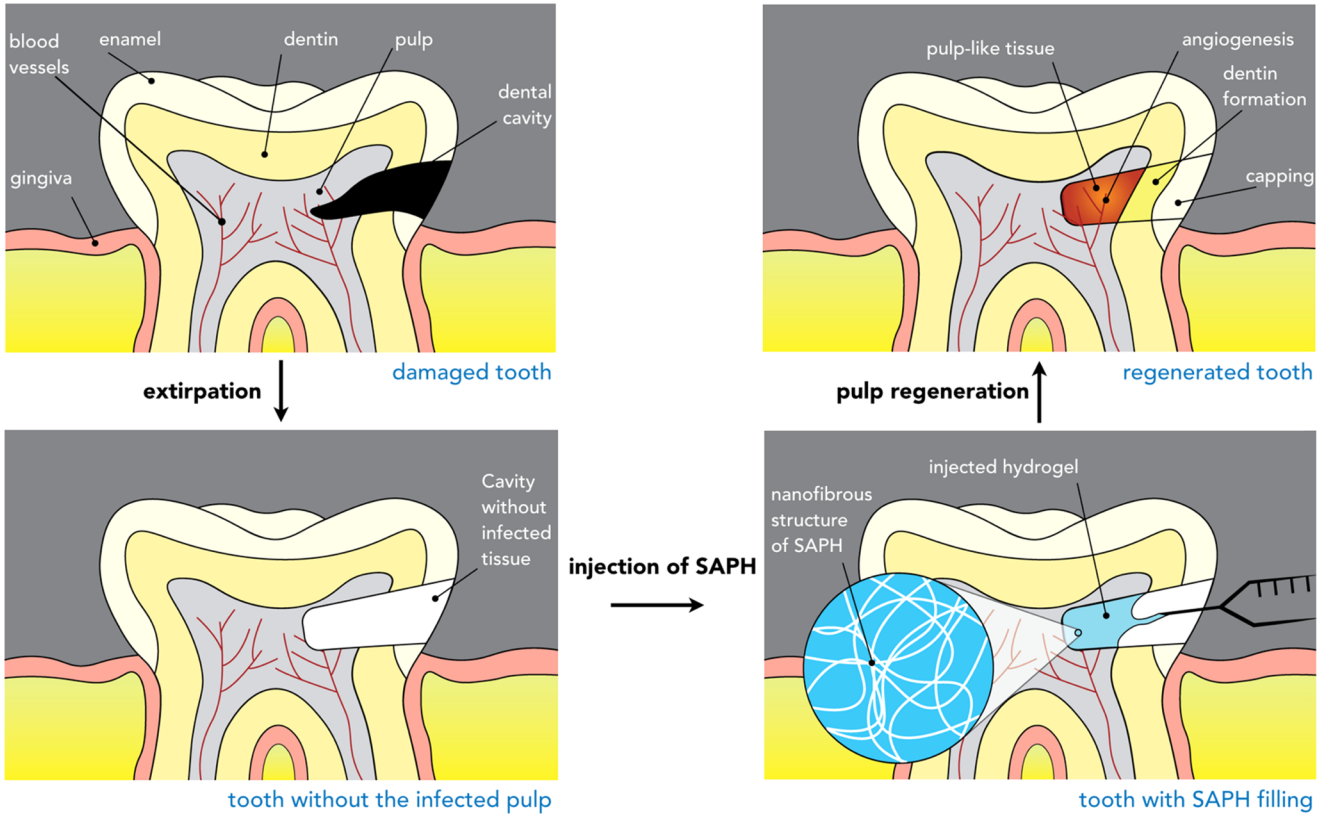

[a]The dental cavity may contain bacterial colonies that need to be extirpated (partial or complete pulpotomy). After clinical extirpation, the void may be filled with the thixotropic peptide hydrogel with dentinogenic activity. As the hydrogel promptly recovers after shear thinning, it should reassemble into a viscoelastic scaffold, filling the void. Recruitment and differentiation of autologous stem cells may then lead to re-establishment of a pulplike tissue niche.

DOI: 10.1021/acsomega.8b00347
ACS Omega 2018, 3, 5980–5987

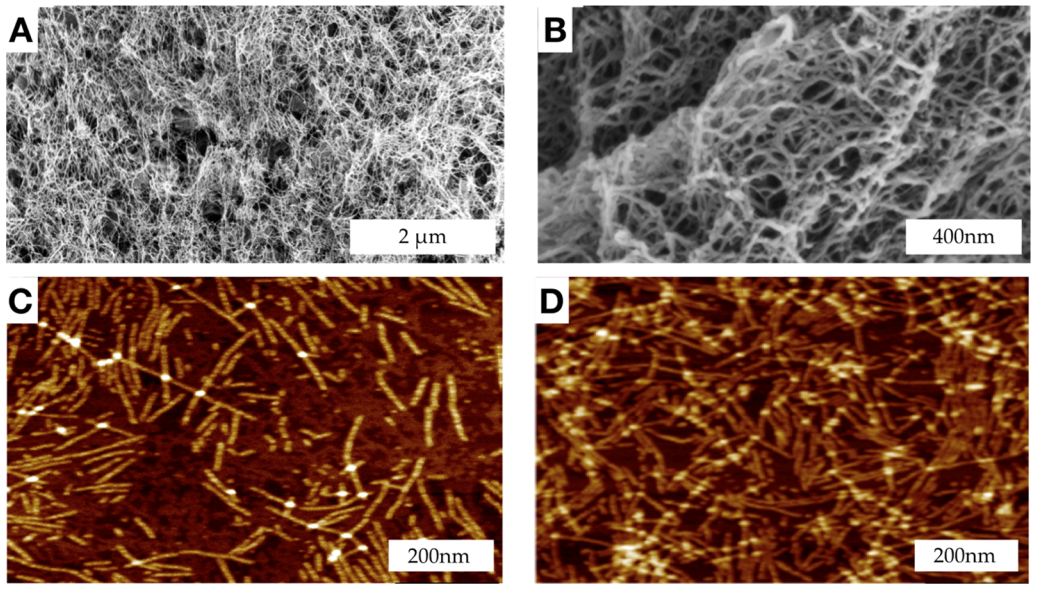

Figure 1. Ultrastructure of the hydrogel formed by SLd. Critical point-dried hydrogel samples in SEM show formation of a dense nanofibrous network with nanoscale pores (A) at low magnification (50k×) and (B) at high magnification (200k×). (C, D) Drop-cast samples of diluted SLd on two-dimensional mica disks show characteristic nanofibrous structure with individual fibers visible in peak force AFM. Measurement of fiber dimensions showed a width of ∼14 nm and a height of ∼2 nm, which is consistent with the proposed self-assembly scenario in Scheme 1.

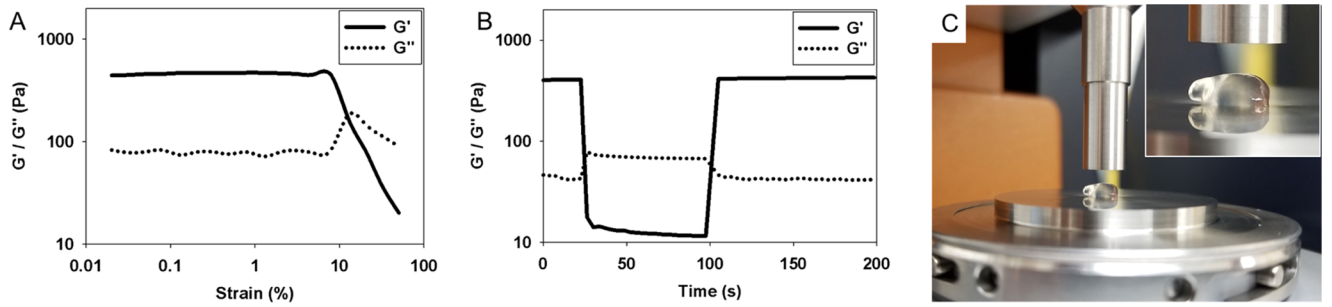

Figure 2. Rheological characterization of hydrogels to demonstrate thixotropy and injectability. (A) Strain sweep of peptide hydrogels show a relatively high storage modulus (G') of about 400 Pa, which is decimated above ∼10% strain. At this point the values for G'' exceed G' indicating liquefaction. (B) Hydrogels are allowed to equilibrate at a constant frequency of 1 Hz and 1% strain rate. As the strain is instantaneously increased to 100%, inversions of G' and G'' occur suggesting instantaneous liquefaction of the gel. Interestingly, after removing the high deformation strain, 100% of the storage modulus is recovered within 3 s. (C) This is evident while pipetting the gel onto the rheometer stage where instantaneous gelation leaves a nubbin suspended with its reflection visible.

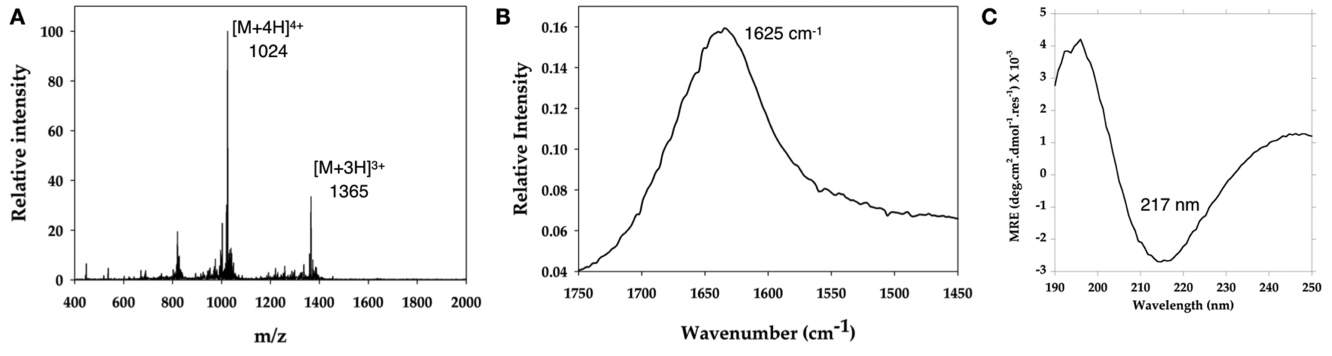

Figure 3. Spectroscopic characterization of the dentinogenic hybrid peptide. (A) Characterization of SLd via mass spectroscopy shows expected $[M + 3H]^{3+}$ and $[M + 4H]^{4+}$ peaks at 1365 and 1024 Da, consistent with the molecular weight (4095 Da). (B) The FTIR spectrum demonstrates the characteristic β-sheet signature peak at 1625 cm^{-1}. (C) Circular dichroism spectrum contains a minimum at 217 nm, which is specific to a β-sheet secondary structure.

from ∼400 to ∼10 Pa, essentially indicating the liquefaction of the gel. When the shear strain is lowered to 1%, the G' of the hydrogel almost instantaneously recovers to ∼400 Pa (Figure 2B). The result can be explained by the noncovalent aspect of the interactions that drive the self-assembly of the nanofibers and the hydrogel. The nanofibrous network that is disrupted by

DOI: 10.1021/acsomega.8b00347
ACS Omega 2018, 3, 5980−5987

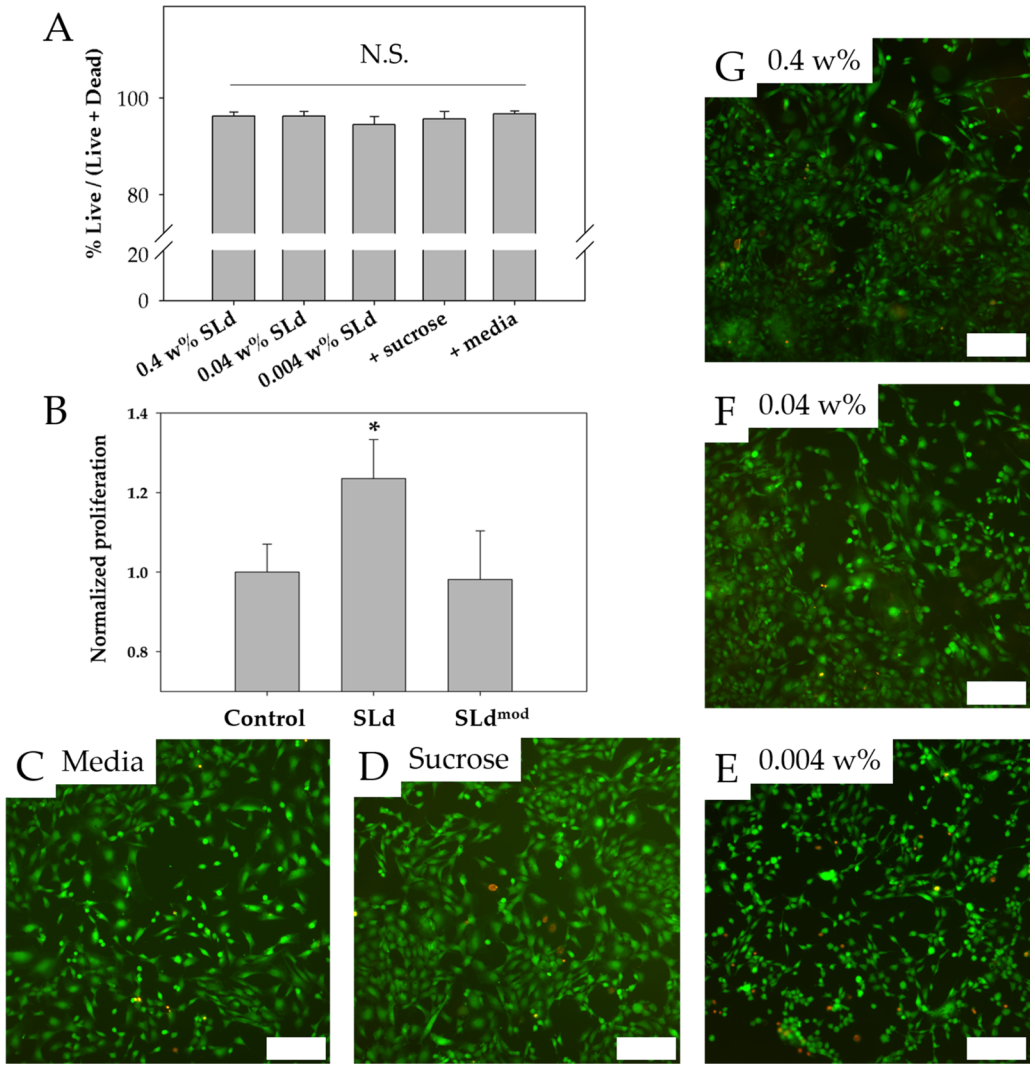

Figure 4. Cytocompatibility and DPSC proliferation. (A) Viability of fibroblasts cultured with SLd at different concentrations (0.004−0.4 wt % w/v), media with formulation solution (298 mM sucrose), or media-only are shown along with their representative live/dead images (C−G). (B) Dental pulp stem cells demonstrated stronger proliferation (CCK-8) compared to no treatment of 0.004 wt % SLd or treatment with a modified variant (SLd^{mod}) with similar charge density (n = 8, *p < 0.01). Scale bar (C−G): 200 μm.

the shear strain can reform when the strain is removed (by reassembly of the hydrogen bond network facilitated by hydrophobic interaction at the nanofiber core), essentially recapitulating the material properties of the nanofibrous mesh. This thixotropic property ensures the injectability of the hydrogel, which meets the requirement of being minimally invasive and easily deliverable. The thixotropic property of the hydrogel is important for formulating a noninvasive protocol to administer the gel to its targeted niche (the dental cavity).

Primary and Secondary Structure. Electrospray ionization mass spectroscopy (ESI-MS) (Figure 3) confirms the identity of the peptide SLd following solid-phase peptide synthesis. The secondary structure of the peptide hydrogel is determined through attenuated total reflectance Fourier-transform infrared spectroscopy (FTIR) and circular dichroism (CD) spectroscopy (Figure 3). The FTIR peak at 1625 cm^{-1} is a signature peak of the amide I band specific to the β-sheet secondary structure and is consistent with the self-assembly scenario depicted in Scheme 1 as well as prior investigations on similar systems.[9,15,17] The CD spectrum, on the other hand, bears the signature β-sheet maximum at 195 nm and minimum at 217 nm.

In Vitro Cytocompatibility and Efficacy. An important first step to evaluate the utility of materials is to determine the cytocompatibility of scaffolds. Fibroblasts were chosen because they are one of the primary cell types found in the dental pulp.[2] We note that SLd scaffolds, regardless of formulation (Figure 4A), show excellent cytocompatibility when compared to media-only and formulation-only (sucrose) controls (Figure 4C,D), over concentrations ranging in 2 orders of magnitude (0.004−0.4 wt %, p < 0.01) (Figure 4E−G). We also show the utility of our conjugation strategy in preserving the proliferative functionality of MEPE, as adult DPSCs proliferate significantly more in response to SLd compared to the control peptide, p < 0.01, (Figure 4B). We have shown that we are able to sustain the viability of fibroblasts and the proliferation of DPSCs in the biodegradable hydrogel that was significantly better than a control (Figure 4). The hydrogel demonstrates a conclusive lack of cytotoxicity in an in vitro environment. Furthermore, injections performed subcutaneously in rats suggest high cytocompatibility in an in vivo environment (data not

DOI: 10.1021/acsomega.8b00347
ACS Omega 2018, 3, 5980−5987

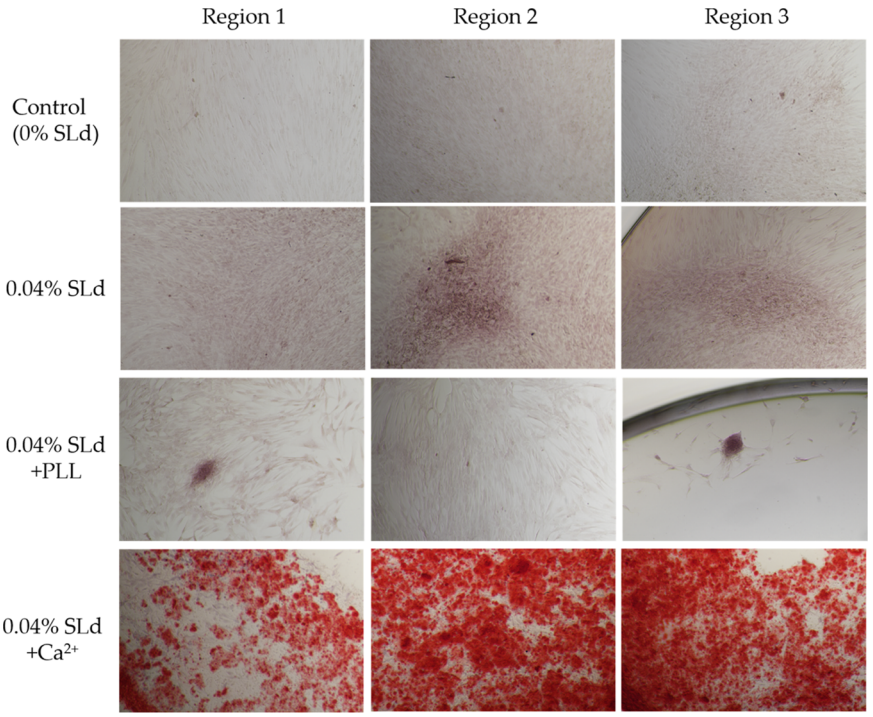

Figure 5. Calcium phosphate deposition in response to SLd treatment of DPSCs (representative regions from independent cultures). SLd hydrogel shows appreciable red staining either alone or in combination with poly-L-lysine (PLL) compared to media-only controls. The addition of Ca^{2+} to the SLd formulation results in significantly more observable calcium phosphate deposition, as observed with Alizarin red staining.

shown) as well as full degradation within 3 days post-implantation (data not shown). We attribute the lack of toxicity to the lack of non-native polymers after degradation and note that similar peptide backbones have been used in the past for tissue regeneration with no record of toxicity.[17,20] The SLd hydrogel that we have developed fulfills our goal of a scaffold that is both nontoxic and encourages DPSC proliferation.

DPSC cultures with SLd show appreciable calcium phosphate deposition compared to their absence in control populations (Figure 5). This demonstrates the ability for the dentonin mimic to stimulate expected biochemical signaling to induce DPSC proliferation and facilitate calcium deposition, essential for robust dentin production. In formulation with $CaCl_2$, SLd self-assembles into signaling platforms for primary DPSC proliferation and robust secondary calcium phosphate deposition. Dentonin additionally has cell adhesion domains with the potential for in vivo recruitment of autologous cells to remodel and deposit biomimetic mineralized matrix.[10]

In summary, while preserving biomimetic nanofibrous architecture (Figure 1), injectability (Figure 2), and secondary structure (Figure 3), the SAPH platform can be modified with bioactive functionality and maintain cytocompatibility (Figures 4 and 5). We demonstrated in vitro that the peptide SLd can self-assemble to form antiparallel β-sheets that stack to form ribbonlike nanofibers (~14 nm wide and ~2 nm high). Noncovalent crosslinking of these nanofibers leads to formation of a robust injectable hydrogel that retains its bioactivity similarly to previous work targeting angiogenesis and immune modulation.[17,18,20,22] Such a platform-app model is especially attractive for β-sheet nanofibers as the functional groups are displayed at a high epitope density along the edge of the nanofiber, which has been shown to be crucial for the bioactivity of similar self-assembled platforms.[21,24]

However, a major drawback of the current construct (SLd) is rapid biodegradation (in vivo), limiting its potential for dental pulp regeneration in its current form. Subcutaneous evaluation of implants in Wistar rats showed rapid degradation over a 1 week period, leaving tissue undiscernible from native cuticular fascia (n = 4, data not shown). Short term (3 days) and long-term (1 week) implants showed similar rapid degradation, which motivated peptide design modification outline in the discussion below. As the next step toward translation, we aim to develop optimized scaffolds that resist degradation for at least 2 weeks.

However, we note the significant stride we made in this study toward supporting dental pulp stem cells in an injectable scaffold, paving the way for a minimally invasive treatment route. For tuning the biodegradation profile, we are currently exploring several modifications to increase the stability of hydrogels in vivo, for example, through insertion of D-amino acids or by increasing the hydrophobicity of the hydrogel. We are currently exploring the modification of the backbone to reduce its susceptibility to matrix metalloproteases by lengthening the SL repeats of the backbone and by altering the charge and polarity of the nanofibers. Finally, peptide hydrogels with similar sequences that have shown to persist in vivo for long term (>2 weeks) can be combined with SLd to manipulate the degradation characteristics and provide prolonged therapeutic function. Another aspect of the regenerative hydrogel we would like to optimize is the ability of the construct to direct angiogenesis from the apical tissue, this would ensure the supply of oxygen and nutrients to the newly developing tissue and prevent the formation of a necrotic core.[17,20] The success of our therapeutic approach would enable the possibility of a regenerative replacement for dental pulp.

DOI: 10.1021/acsomega.8b00347
ACS Omega 2018, 3, 5980−5987

CONCLUSIONS AND OUTLOOK

The ability to regenerate the dental pulp is a critical breakthrough required to preserve the vitality of teeth following root canal therapies. In this study, we engineered a minimally invasive injectable peptide scaffold and demonstrate the feasibility of this functionalized self-assembled platform to support dental pulp stem cells and stromal cells in a biomimetic hydrogel environment. Specifically, we demonstrate the injectable properties crucial for clinical application, and we show the potential of SLd to support proliferation of DPSCs and increase calcium phosphate deposition while also exhibiting cytocompatibility to other critical stromal cells found in the dental pulp. The results demonstrate the first steps in improving the standard of care for root canal therapies. The next step in peptide modification would be aimed at tuning the biodegradability of the hydrogels in vivo. We will optimize the SAPH system for in vivo disease models (partial pulpotomy in dog models) to further showcase the viability of such a biomimetic tissue regeneration approach. Replacement of inert seals in dental cavities with an engineered bioresponsive matrix to promote vital pulplike tissue regeneration would be a major step forward for nanomedicine and dental tissue engineering.

EXPERIMENTAL SECTION

Peptide Synthesis and Preparation. The peptides described in Table 1 were synthesized using a solid-phase peptide synthesis protocol modified from methods previously published with acetyl N-terminal and amide C-terminal protective groups.[15,17,20] All amino acids, resin, and coupling reagents were purchased from CEM Corporation. Standard solid-phase peptide synthesis was performed using a CEM Liberty Blue microwave peptide synthesizer and Rink amide resin with 0.18 mmol/g loading. Following synthesis, each peptide was cleaved from the resin and the crude mass was checked prior to dialysis against deionized water with 2000 Da molecular weight cut-off dialysis tubing (Cole-Parmer). The peptides were then lyophilized, and their purity was measured using electron-spray ionization mass spectrometry (Bruker Instruments). Peptides were reconstituted in sterile 298 mM sucrose solution (Sigma-Aldrich) and gelation of the peptides into thixotropic hydrogels was performed by the addition of a molar equivalent of calcium chloride (Sigma-Aldrich) to balance the overall negative charge of the peptides.

Peptide Characterization. Scanning electron microscopy (SEM), atomic force microscopy (AFM), rheology, and Fourier-transform infrared spectroscopy (FTIR) were performed as previously described.[15,17,18,20,22] For SEM, hydrogel samples were fixed in glutaraldehyde, ethanol dehydrated, critical point dried, sputter coated with gold/palladium, and imaged on a field emission SEM (LEO 1530VP). For AFM, the peptide solutions (0.01−0.05 wt %) were spin-coated onto clean mica disks. Images were collected on a Dimension Icon AFM (Bruker Instruments) in ScanAsyst mode. For rheology, 4 wt % solution of peptide hydrogel was transferred onto an 8 mm parallel plate geometry with a gap of 250 μm. Strain sweep (0−1000% strain at 1 Hz) and shear recovery (1% strain at 1 Hz for 20 s, 100% strain at 1 Hz for 60 s, and 1% strain at 1 Hz for 120 s) were performed using an ARES-G2 rheometer (TA Instruments). For FTIR, the peptide solutions (0.04 wt %) were pipetted onto a universal attenuated total reflectance accessory and dried until a thin film of peptide was achieved. Infrared spectrum was taken using a Spectrum 100 FTIR spectrometer (PerkinElmer). For circular dichroism, we used an Olis Rapid Scanning Monochromator to measure the ellipticity of a 0.004% peptide solution from 190 to 250 nm in a 1 cm cuvette. The ellipticity (θ, measured in millidegrees) was converted to molar residual ellipticity (θ) according to the formula: $(\theta) = (\theta \cdot m)/(10 \cdot cln)$, where m is the molecular weight of the peptide, c is the concentration of the peptide solution in mg/mL, l is the path length of the cuvette in centimeter, and n is the no. of residues in the peptide sequence (similar to calculations described before).[25]

In Vitro Cytocompatibility. All reagents and materials were purchased from Fisher Scientific unless otherwise noted. Mouse 3T3 fibroblasts (NIH) were cultured in media (Dulbecco's modified Eagle medium supplemented with 10% fetal bovine serum and 1% 100× penicillin streptomycin) in T75 flasks. Media was changed every 3 days until the fibroblasts reached confluency. For cytocompatibility studies, fibroblasts were seeded in a 96-well plate (5000 cells/well). Three conditions (0.4, 0.04, and 0.004 wt % SLd; $n = 6$) and two controls (media with sucrose and media alone; $n = 6$) were tested. For each condition, the specified amount of peptide was supplemented in the media, and for the media control with sucrose, 298 mM sucrose was supplemented to the media corresponding to the amount added to the tested conditions. Media was changed daily and cytocompatibility was assessed on day 3 using a LIVE/DEAD Viability/Cytotoxicity kit. Images were taken on an Eclipse Ti-S inverted microscope (Nikon Instruments). Cell viability was quantified using ImageJ (NIH).

In Vitro Proliferation and Efficacy. DPSCs (Lonza) were cultured using a DPSC BulletKit (Lonza) in T75 flasks. Media was changed every 3 days. For the proliferation assay, cells were seeded into 96-well plates (5000 cells/well). Media and 0.004 wt % SLd^{mod} were used as controls ($n = 8$), whereas the tested condition contained 0.004 wt % SLd ($n = 8$). Media was changed daily and proliferation was evaluated on day 3 using the Cell Counting Kit-8 (CCK-8, Dojindo). Using an Infinite m200 PRO plate reader (Tecan) with the temperature set to 37 °C, initial absorbance was measured at 450 nm (reference wavelength: 650 nm). For the calcium deposition assay, DPSCs were seeded in 96-well plates (5000 cells/well) with $n = 3$ for each condition. Three conditions were tested (0.04, 0.04 wt % SLd with ε-poly-L-lysine (PLL, Carbosynth), and 0.04 wt % SLd with Ca^{2+}) against a control without SLd. Conditions with PLL and Ca^{2+} had equal molar equivalents added to balance the overall charge of the peptide. Cells were cultured in differentiation media (proliferation media supplemented with 50 μg/mL ascorbic acid, 10 nM dexamethasone, and 10 mM β-glycerophosphate) for 2 weeks. Cells were stained with Alizarin Red S (Sigma-Aldrich) on day 14 and imaged with an Eclipse Ti-S inverted microscope to observe calcium deposition.

In Vivo Subcutaneous Implantation. All animal studies were approved by the NJIT-Rutgers animal care and use committee. Female Wistar rats (225−250 g, Charles River Labs) were prepped and injected subcutaneously in the dorsal region with 200 μL of peptide hydrogel, with each rat receiving a total of four implants ($n = 4$). At the specified time points (3 day and 1 week), the rats were sacrificed and regions around the implant were excised, fixed, and processed for routine histological staining.

Statistical Analysis. Results are presented as mean ± standard deviation. Comparisons were made using analysis of variance (ANOVA) for multiple comparisons with Tukey post hoc analysis for parametric data. Nonparametric tests were

DOI: 10.1021/acsomega.8b00347
ACS Omega 2018, 3, 5980−5987

carried out using the Kruskal–Wallis ANOVA with Dunn's post hoc analysis. Statistical significance was accepted for $p < 0.01$.

AUTHOR INFORMATION

Corresponding Authors

*E-mail: biplab.sarkar@njit.edu (B.S.).
*E-mail: vak@njit.edu (V.A.K.).

ORCID

Biplab Sarkar: 0000-0002-9298-2392
Vivek A. Kumar: 0000-0001-7536-9281

Author Contributions

The manuscript was written through contributions of all authors. All authors have given approval to the final version of the manuscript.

Notes

The authors declare no competing financial interest.

ACKNOWLEDGMENTS

We would like to acknowledge NJIT for their startup fund and faculty seed grant support. We would also like to acknowledge NJIT for their support by awarding us two Undergraduate Research Innovation (URI) seed grants and a Provost Summer URI Fellowship. We sincerely thank Stephen D. Kozuch and Prof. David Sabatino at Seton Hall University for help with circular dichroism.

ABBREVIATIONS

SAPH, self-assembling peptide hydrogel; DPSC, dental pulp stem cell; SEM, scanning electron microscopy; AFM, atomic force microscopy; MEPE, matrix extracellular phosphoglycoprotein; ECM, extracellular matrix; VEGF, vascular endothelial growth factor; ESI-MS, electrospray ionization mass spectroscopy; FTIR, Fourier-transform infrared spectroscopy

REFERENCES

(1) Dye, B.; Thornton-Evans, G.; Li, X.; Iafolla, T. Dental Caries and Tooth Loss in Adults in the United States, 2011–2012. In *NCHS Data Brief No. 197*; National Center for Health Statistics: Hyattsville, MD, 2015.

(2) Gulabivala, K.; Ng, Y. L. 1 - Tooth Organogenesis, Morphology and Physiology. In *Endodontics*, 4th ed.; Mosby, 2014; pp 2–32.

(3) Ostby, B. N. The role of the blood clot in endodontic therapy. An experimental histologic study. *Acta Odontol. Scand.* **1961**, *19*, 324–353.

(4) Myers, W. C.; Fountain, S. B. Dental pulp regeneration aided by blood and blood substitutes after experimentally induced periapical infection. *Oral Surg., Oral Med., Oral Pathol.* **1974**, *37*, 441–50.

(5) Huang, G. T. Pulp and dentin tissue engineering and regeneration: current progress. *Regener. Med.* **2009**, *4*, 697–707.

(6) Mooney, D. J.; Powell, C.; Piana, J.; Rutherford, B. Engineering dental pulp-like tissue in vitro. *Biotechnol. Prog.* **1996**, *12*, 865–868.

(7) Bohl, K. S.; Shon, J.; Rutherford, B.; Mooney, D. J. Role of synthetic extracellular matrix in development of engineered dental pulp. *J. Biomater. Sci., Polym. Ed.* **1998**, *9*, 749–764.

(8) About, I.; Mitsiadis, T. A. Molecular aspects of tooth pathogenesis and repair: in vivo and in vitro models. *Adv. Dent. Res.* **2001**, *15*, 59–62.

(9) Galler, K. M.; Aulisa, L.; Regan, K. R.; D'Souza, R. N.; Hartgerink, J. D. Self-assembling multidomain peptide hydrogels: designed susceptibility to enzymatic cleavage allows enhanced cell migration and spreading. *J. Am. Chem. Soc.* **2010**, *132*, 3217–3223.

(10) Liu, H.; Li, W.; Gao, C.; Kumagai, Y.; Blacher, R. W.; DenBesten, P. K. Dentonin, a fragment of MEPE, enhanced dental pulp stem cell proliferation. *J. Dent. Res.* **2004**, *83*, 496–499.

(11) Six, N.; Septier, D.; Chaussain-Miller, C.; Blacher, R.; DenBesten, P.; Goldberg, M. Dentonin, a MEPE fragment, initiates pulp-healing response to injury. *J. Dent. Res.* **2007**, *86*, 780–785.

(12) Moore, A. N.; Lopez Silva, T. L.; Carrejo, N. C.; Origel Marmolejo, C. A.; Li, I. C.; Hartgerink, J. D. Nanofibrous peptide hydrogel elicits angiogenesis and neurogenesis without drugs, proteins, or cells. *Biomaterials* **2018**, *161*, 154–163.

(13) Aulisa, L.; Dong, H.; Hartgerink, J. D. Self-assembly of multidomain peptides: sequence variation allows control over cross-linking and viscoelasticity. *Biomacromolecules* **2009**, *10*, 2694–2698.

(14) Moore, A. N.; Hartgerink, J. D. Self-Assembling Multidomain Peptide Nanofibers for Delivery of Bioactive Molecules and Tissue Regeneration. *Acc. Chem. Res.* **2017**, *50*, 714–722.

(15) Dong, H.; Paramonov, S. E.; Aulisa, L.; Bakota, E. L.; Hartgerink, J. D. Self-assembly of multidomain peptides: balancing molecular frustration controls conformation and nanostructure. *J. Am. Chem. Soc.* **2007**, *129*, 12468–12472.

(16) Bakota, E. L.; Wang, Y.; Danesh, F. R.; Hartgerink, J. D. Injectable multidomain peptide nanofiber hydrogel as a delivery agent for stem cell secretome. *Biomacromolecules* **2011**, *12*, 1651–1657.

(17) Kumar, V. A.; Taylor, N. L.; Shi, S.; Wang, B. K.; Jalan, A. A.; Kang, M. K.; Wickremasinghe, N. C.; Hartgerink, J. D. Highly angiogenic peptide nanofibers. *ACS Nano* **2015**, *9*, 860–868.

(18) Kumar, V. A.; Taylor, N. L.; Shi, S.; Wickremasinghe, N. C.; D'Souza, R. N.; Hartgerink, J. D. Self-assembling multidomain peptides tailor biological responses through biphasic release. *Biomaterials* **2015**, *52*, 71–78.

(19) Wang, Y.; Bakota, E.; Chang, B. H.; Entman, M.; Hartgerink, J. D.; Danesh, F. R. Peptide nanofibers preconditioned with stem cell secretome are renoprotective. *J. Am. Soc. Nephrol.* **2011**, *22*, 704–717.

(20) Kumar, V. A.; Liu, Q.; Wickremasinghe, N. C.; Shi, S.; Cornwright, T. T.; Deng, Y.; Azares, A.; Moore, A. N.; Acevedo-Jake, A. M.; Agudo, N. R.; Pan, S.; Woodside, D. G.; Vanderslice, P.; Willerson, J. T.; Dixon, R. A.; Hartgerink, J. D. Treatment of hind limb ischemia using angiogenic peptide nanofibers. *Biomaterials* **2016**, *98*, 113–119.

(21) Cui, H.; Webber, M. J.; Stupp, S. I. Self-assembly of peptide amphiphiles: from molecules to nanostructures to biomaterials. *Biopolymers* **2010**, *94*, 1–18.

(22) Kumar, V. A.; Shi, S.; Wang, B. K.; Li, I. C.; Jalan, A. A.; Sarkar, B.; Wickremasinghe, N. C.; Hartgerink, J. D. Drug-triggered and cross-linked self-assembling nanofibrous hydrogels. *J. Am. Chem. Soc.* **2015**, *137*, 4823–4830.

(23) Brizuela, C.; Ormeno, A.; Cabrera, C.; Cabezas, R.; Silva, C. I.; Ramirez, V.; Mercade, M. Direct Pulp Capping with Calcium Hydroxide, Mineral Trioxide Aggregate, and Biodentine in Permanent Young Teeth with Caries: A Randomized Clinical Trial. *J. Endod.* **2017**, *43*, 1776–1780.

(24) Webber, M. J.; Tongers, J.; Newcomb, C. J.; Marquardt, K. T.; Bauersachs, J.; Losordo, D. W.; Stupp, S. I. Supramolecular nanostructures that mimic VEGF as a strategy for ischemic tissue repair. *Proc. Natl. Acad. Sci. U.S.A.* **2011**, *108*, 13438–13443.

(25) Sarkar, B.; O'Leary, L. E.; Hartgerink, J. D. Self-assembly of fiber-forming collagen mimetic peptides controlled by triple-helical nucleation. *J. Am. Chem. Soc.* **2014**, *136*, 14417–14424.

DOI: 10.1021/acsomega.8b00347
ACS Omega 2018, 3, 5980–5987